Exploring the Feasibility of Solid-Fuel Use in a Turbojet Engine for Reduction of Mechanical Complexity

Guy Bayan

Science Leadership Academy Engineering

John Kamal

May 13, 2022

Abstract

As a method of air-breathing propulsion, turbojet engines have the advantage of being highly efficient, but this comes at the cost of mechanical complexity and consequently high manufacturing price. With this in mind, the primary goal of this project was to explore the ways in which turbojet complexity could be reduced while still maintaining high levels of efficiency. This was done by researching the principles on which turbojets operated, identifying the causes of fuel efficiency as well as the conditions necessary for combustion. A design was hypothesized that utilized solid fuel with a weak chemical oxidizer, in theory allowing for compressor efficiency to be low while still achieving combustion. Because it was unknown whether a partial chemically-oxidized fuel could still be further oxidized by compressed air, several preliminary tests were conducted. The results showed that this was possible, supporting the feasibility of this engine and allowing the experiment to continue. The next step was to test whether a partially-oxidized fuel could solely sustain compressor start-up, as this would precede atmospheric oxidation and the combustion would be inherently weak. A solid-fuel turbine was

designed and built, being designated as Prototype 1. In addition to testing deoxygenated compressor start-up, Prototype 1 demonstrated whether the simple materials used in construction could withstand the extreme conditions of a turbojet engine. The results of the test revealed that the turbine accelerated to 6,300 RPM in 2.33 seconds, proving the feasibility of deoxygenated start-up. As for the materials used in construction, all remained undamaged with an exception of the J-B Weld adhesive, which failed drastically in multiple areas due to the high heat. This ultimately caused the turboshaft rotation to be cut short, though valuable data was still recovered. Overall, the performance of Prototype 1 was considered to be very successful, surpassing expectations.

Introduction

Of the many types of aerospace propulsion methods that are available, some are more commonly used than others. The turbojet engine is one of the most popular examples, with its incredibly high fuel efficiency derived from the use of atmospheric oxygen instead of a chemical oxidizer. It is an ideal engine type for in-atmosphere travel, but comes at the expense of mechanical complexity and the resultantly high cost for manufacturing. Another popular propulsion system is the solid-fuel rocket motor, ideally suited for unmanned hypersonic payloads. With its extremely low manufacturing cost compared to other engines with similar thrust outputs, it has remained popular since its invention in the 13th century. Unfortunately, solid-fuel rockets have the lowest efficiency of any aerospace propulsion method, with a maximum specific impulse of 250 seconds.

When conducting this study, the primary question being asked was, “Is it possible to design and create an engine that incorporates the efficiency of a turbojet engine with the

mechanical simplicity of a solid rocket motor?" Though measuring the efficiency of the engine is not intended in this study due to logistical constraints, it is hypothesized that the incorporation of an air breathing component in a solid-fuel rocket would cause a 50% - 100% increase in specific impulse (efficiency). Using a typical industrial solid-fuel composition, this could lead to a specific impulse of up to 500 seconds. Being able to achieve this could prove to be revolutionary in the aerospace industry, as it would allow for relatively high-efficiency single use engines, a role that has never been filled. This can be seen in the gap between rockets and air-breathing engines graphed on "Propulsion Performance" (Kashkhan, 2009). If developed further, modified versions of this engine could even bridge the gap between air travel and space travel, similar to what was being attempted by the SABRE engine (Nallard, 2020). The main goal of this study, however, is the attempt to create an economical but efficient propulsion system for aircraft.

When attempting to design a simplified turbojet engine, it is necessary to understand what conditions must be met for combustion to be sustained. Because the fuel typically used in jet engines is energy-dense and therefore difficult to combust, the flow conditions required in a jet engine are extremely specific as well as difficult to achieve. (Jet engine pressure distribution) It was hypothesized that if a fuel could be used that didn't rely solely on the ideal flow of compressed air, the design tolerances could be loosened, reducing manufacturing cost. It was then realized that this sort of independence from compressed air could be accomplished through the incorporation of a chemical oxidizer. The chemical oxidizer could allow the compressors to be less efficient while still maintaining the combustion necessary to keep them operating as a useful component of the combustion cycle. Without self-sustaining compression and combustion, the engine could not be considered a true turbojet engine, which is why a constant source of

oxidation could prove to be so vital. Through this reasoning, the disposable aircraft solid-fuel turbojet (DAST) engine was conceived.

Methods

After identifying the principles on which the DAST engine would rely, a basic physical design for it was brainstormed. After the design of the engine was outlined conceptually, a diagram of it was drafted, (fig. 1) though it was still relatively undeveloped. The DAST engine would be best described as a hybrid between a solid fuel rocket motor and a turbojet engine. Fundamentally, its construction would consist of a simple sheet metal cylinder with two sets of struts on either end intended to support the turboshaft. The turboshaft likely would be built around a steel rod with structural ribs placed along its length to provide a converging-diverging form necessary for the compression of air and the expansion of exhaust gasses. A number of axial compressors and one turbine would also be placed along the length of the shaft, with an annular fuel grain situated between them. In theory, an electrically activated pyrotechnic igniter placed slightly forward of the fuel grain should initiate “deoxygenated combustion.” In this stage, the fuel combustion would not rely on atmospheric oxygen, but primarily on a chemical oxidizer. The fuel mixture, which would likely consist of 1 part potassium nitrate (KNO_3) and 2 parts sugar, by mass, is weakly oxidized compared to the ideal ratio for combustion of 2 parts potassium nitrate to 1 part sugar. The reason for this is that turbojets derive their high efficiency values from the use of atmospheric oxygen, which is not carried supplementally to the fuel. Relying entirely on a chemical oxidizer would be inferior in terms of efficiency due to the additional oxidiser mass required to attain similar total impulse, and would result in low specific impulse values similar to that of a solid rocket motor. The weakly-oxidized fuel would cause a

low initial burn rate, but would also produce copious amounts of heat and exhaust gases. These gases would spin the turbine and the connected compressors to speeds sufficient for self-sustaining combustion. To prevent the exhaust gasses from back-flowing through the engine, a 3D printed intake cover would be utilized. After the turbine reaches this threshold speed, an electrical ignitor would detonate a black powder separation charge in the cover, blowing it from the engine. This would then allow the intake and compression of air, intensifying combustion in the engine, and further accelerating the speed of the turbine and compressors. This increasing burn rate and combustion efficiency would consequently boost the thrust output of the engine. After the fuel grain has been fully consumed, the combustion would cease and the compressors would subsequently spin down to 0 RPM. If refueling of the engine was found to be practical, a replacement fuel grain and ignitors would be required, as well as partial disassembly – specifically of the turboshaft and turboshaft struts.

The chemical oxidizer incorporated in the DAST engine fuel grain could provide three benefits over traditional turbojet engines. First, the engine wouldn't require an APU (auxiliary power unit) to initiate the compressor spin-up before combustion. Second, it would allow the process of compression to be less efficient while still maintaining self-sufficiency through combustion, which is the primary goal of this study. This means that manufacturing tolerances wouldn't have to be as precise, leading to a reduction in cost and required resources. And finally, it could allow the engine to function at extremely high altitudes with minimal reduction in efficiency. This is due to combustion not relying entirely on atmospheric oxygen, as in traditional jet engines.

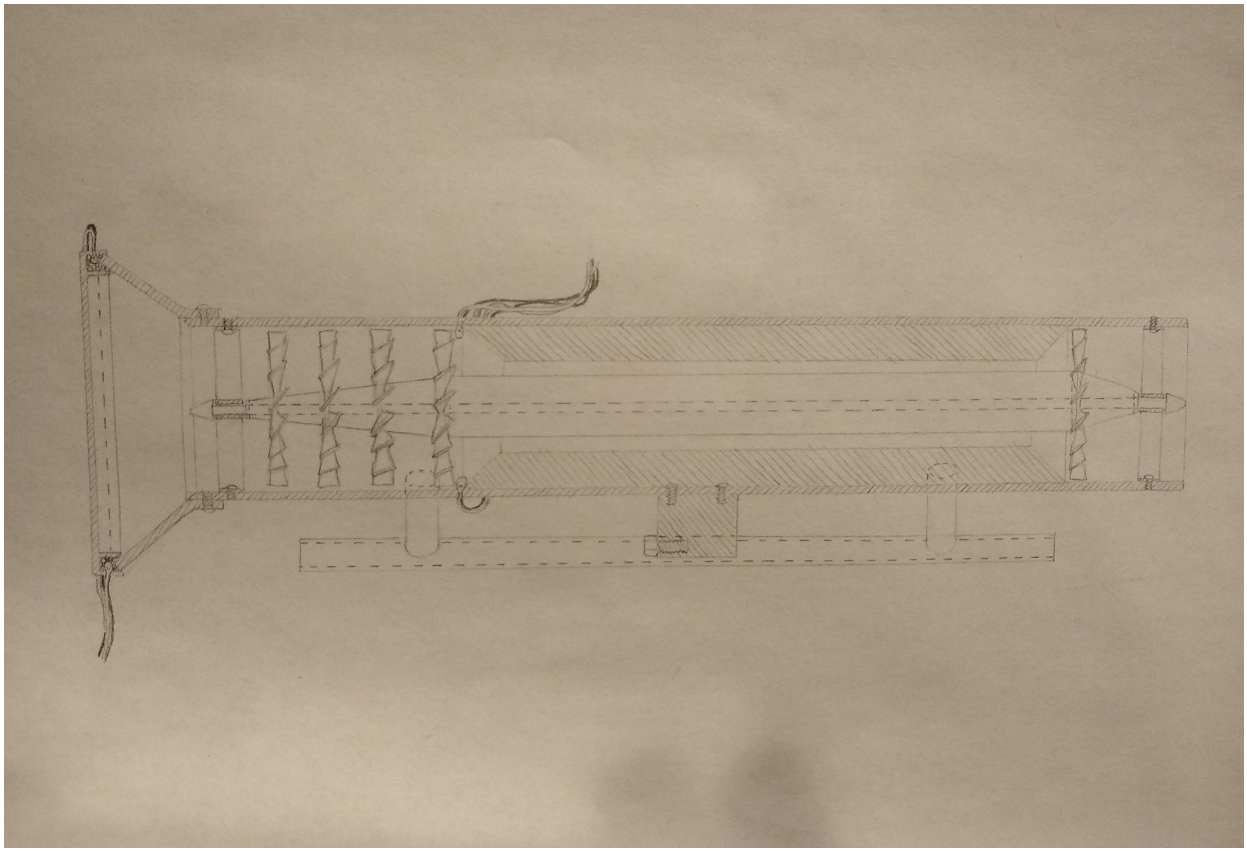

Figure 1.

One of the initial diagrams of the DAST engine drafted before preliminary experimentation and result analysis.

While it was hypothesized that the DAST engine would succeed in achieving self-sustaining combustion, there were also many concerns over different aspects of the design. Through the research of flow dynamics (High speed aerodynamics) and turbine-specific flow, (Jet engine pressure distribution) several specific reasons for failure were identified, though purely structural failures were neglected due to being an issue of construction rather than concept:

- Initial fuel ignition doesn't start.
- Initial deoxygenated burn doesn't spin up the compressor to sufficient speeds.
- Initial deoxygenated burn takes too long to spin up the compressor.
- Intake cover separates too soon due to high combustion chamber pressure.
- Intake cover melts due to high combustion chamber temperature.
- Intake cover separation charge fires too soon due to high combustion chamber temperature.
- Intake cover doesn't separate due to vacuum created by the compressor.
- Combustion back flows through engine immediately after cover separation, terminating compressor movement and thrust.
- Combustion suffocates due to a lack of compressor efficiency.
- Intake air speed too fast for compression to occur. (due to Bernoulli's Principle)
- Intake air speed too fast for combustion to occur. (flameout)
- Combustion chamber too constricted to sustain fuel oxidation.
- Fuel grain surface area too large/incorrectly shaped to oxidize evenly.
- Flame front and gas expansion too far from the turbine for optimal efficiency.
- Changing fuel grain shape causes a drop in combustion chamber pressure.

While most of these scenarios stem from combustion issues, a fair quantity are derived from intake cover failures, alone. This factor would contribute to a design change further on in the experiment.

Because the DAST engine would rely on several principles which were largely untested by the scientific community, several preliminary tests were required. The main purpose of these

tests was to determine the feasibility of the experimental principles in allowing the engine to function, and included concepts such as two-source fuel oxidation (Preliminary test 2), and deoxygenated compressor start-up (Prototype 1). These preliminary tests would also aid in revision of the final engine design, making them extremely significant to the overall experiment. This would be achieved through meticulous experimental design and analysis of results, as design flaws that remain unexposed by the tests could lead to major failures in future prototypes.

Preliminary Test 1: Coarse Vs. Fine Fuel Components

Scientific question: Does milling the fuel components before melting them down affect the burn rate/efficiency?

Hypothesis: Milling the fuel components beforehand would have little to no effect on the burn rate.

Variables: Burn rate with milled fuel components and coarse fuel components.

Methods: 2 grams of potassium nitrate were combined with 1 gram of confectioner's sugar and melted down in a stovetop container. The mixture was poured into a mold and left to set. The fuel grain was ignited and the burn recorded on video. Burn characteristics and byproducts were noted. 2 grams of potassium nitrate were combined with 1 gram of confectioner's sugar and milled down in a mortar and pestle (to roughly 10 μm particles). The

mixture was then melted down in a stovetop container, poured into a mold and left to set. The fuel grain was ignited and the burn recorded on video. Burn characteristics and byproducts were noted.

Results: The coarse fuel grain, which took on a light brown color, burned consistently and strongly for approximately 7 seconds. Minimal byproducts were produced by the burn. The milled fuel grain, which unexpectedly took on a gray color after being melted, defligrated very rapidly for about 2 seconds. This disproved the hypothesis that the burn rate wouldn't be affected. The milled fuel burn seemed more efficient, however, the coarse fuel may still be preferred over the milled fuel due to added stability. Fuel deflagration that is too rapid would also prevent the turbine from accelerating to sufficient speeds for compression.

Though not originally intended, a third variable was also tested to see if there would be any variation in the results. 2 grams of potassium nitrate was milled down separately from the sugar in a mortar and pestle. The potassium nitrate was stirred into 1 gram of confectioner's sugar and melted down in a stovetop container. The final mixture took on a gray color, similar to the mixture with the fuel components milled together. This mixture burned very rapidly, possibly even more so than when the fuel components were milled together. This further supports the idea that the use of fine or coarse fuel has a huge effect on burn rate, even when melted down.

Preliminary Test 2: Two-Source Fuel Oxidation

Scientific question: Is it possible for fuel with a weak chemical oxidizer to have an additional source of oxidation for fuel combustion? - Does introducing airflow around a weak oxidizer-assisted deflagration increase the burn rate?

Hypothesis: Introducing airflow to a weakly-oxidized fuel does increase the burn rate.

Variables: Burn rate with airflow and burn rate without airflow, 1:1 oxidizer-fuel ratio and 1:2 oxidizer-fuel ratio.

Methods: 1.5 grams of potassium nitrate were milled with a mortar and pestle (to approximately 10 μm particles), combined with 1.5 grams of confectioners sugar, and melted down on a stovetop container. The mixture was poured into a mold, left to set, and the mass of the final product was recorded. The fuel grain was then ignited and allowed to burn uninterrupted. When the unassisted burn duration was recorded, the experimenter repeated the first several steps of the experiment but blew on the burning fuel grain for the entirety of the test, recording the burn duration. 1 gram of potassium nitrate was milled in a mortar and pestle, combined with 2 grams of confectioners sugar, and melted down on a stovetop container. The mixture was poured into a mold and left to set, and the mass of the final product was recorded. The fuel grain was then ignited and allowed to burn uninterrupted. When the unassisted burn duration had been recorded, the experimenter casted and weighed a new fuel grain, but blew on it for the entirety of the test, recording the burn duration. The burn rates were calculated from the

data and the two different fuel ratio tests were compared to each other to see if one ratio was more heavily affected by airflow than the other.

Results: Through initial testing, it was realized that when a small ratio of oxidizer to fuel is used in an unmilled mixture, it leads to an extremely slow and uneven burn rate, with many solid byproducts left behind. In a turbojet engine, this could be especially detrimental, as it could cause excessive damage to the turbine blades. For this reason, it was decided that the potassium nitrate would be milled before being combined with the sugar.

Table 1.

Experimental data collected on two-source oxidation compared to exclusively chemical oxidation.

Independent variables	Fuel grain mass (g)	Burn duration (s)	Burn rate (g/s)	Airflow / no airflow ratio
1:1, no airflow	2.08	11	0.189	1.31
1:1, airflow	2.48	10	0.248	
2:3, no airflow	1.73	24	0.072	0.78
2:3, airflow	2.12	38	0.056	
1:2, no airflow	2.32	61	0.037	N/A
1:2, airflow	2.15	N/A	N/A	

The first fuel grain to be made during this experiment, which was meant to be a test of the “1:1, no airflow” variable, had a chunky texture due to a low heating temperature. This would later prove to have a large effect on the burn rate. When the fuel grain made for variable “1:1, airflow,” was tested, there seemed to be a clear response to the increased airflow (see fig. 2

and fig. 3), but when the burn rate was calculated, it was found to be comparable to the “no airflow” test, disagreeing with the hypothesis. Believing there to be a mistake in the results, a new fuel grain was made for the “1:1, no airflow” variable, this time ensuring that the fuel mixture had been completely melted down and was no longer lumpy. This time, the burn rate was substantially lower, possibly indicating that fuel with unmelted particles has a higher burn rate because more surface area is available for combustion. It is important to note that airflow was not sustained for the entire duration of the airflow tests because the experimenter had to inhale. On the second day of the experiment, when both 1:2 variables were scheduled to be tested, it was decided that the tests would be done indoors due to inclement weather. First, was the 1:2, no airflow test, which took an astounding 61 seconds to burn and extinguish itself, indicating an extremely low burn rate. When calculated, the 0.037 g/s burn rate was approximately 5 times lower than the 1:1, no airflow test, showing that the amount of oxidizer incorporated into the fuel grain has an exponential effect on the burn rate - a relationship that was not previously considered. When an airflow was introduced to the 1:2 mixture, it ultimately extinguished the flame which was already weak to begin with. This was likely due to the low combustion temperature of the weakly oxidized mixture, which would have been lowered even further by the increased airflow. Because of this drastic difference between the 1:1 mixture burn rate and the 1:2 mixture burn rate, a third mixture was introduced into the experiment. The 2:3 mixture would have an oxidizer amount halfway between the two previous mixtures, and presumably an intermediate burn rate. As expected, when the 2:3, no airflow variable was tested it had an intermediate burn rate of 0.072 g/s, however, when the 2:3, airflow variable was tested, the burn rate decreased by a fair margin, as in the 1:2, airflow test, though not extinguishing

completely. The video footage seemed to confirm the earlier hypothesis that airflow reduced the burn rate by removing heat from an already weak combustion.

Figure 2.

Photograph of fuel grain combustion, normally.

Figure 3.

Photograph of fuel grain combustion during airflow.

The findings of this experiment show that the most optimal fuel ratio for use in a turbojet is 1:1, firstly because of its readiness to be oxidized by external airflow, and secondly because of its high combustion temperatures. This gives it better resistance to being extinguished by high-velocity airflow than its more weakly-oxidized counterparts, which is a necessary attribute in a turbojet engine.

Preliminary Test 3: Intake Cover Heat Resistance

Scientific question: Would a 3-D printed intake cover be able to withstand the temperatures of combustion for the duration of compressor start-up?

Hypothesis: A 3-D printed intake cover would not be able to withstand the temperatures of combustion for long enough and would melt through in less than 5 seconds.

Variables: Amount of time to melt through ABS plastic, Carbon fiber plastic.

Methods: Two disks, one made from ABS plastic and the other made of carbon fiber plastic, were printed in a 3-D printer. Both disks were about 5 mm thick and 4 cm wide. The ABS plastic disk was propped up against a non-flammable surface and a butane torch flame was directed at the disk from 5 cm away. The time from ignition of the torch to disk penetration was recorded. Next, the carbon fiber plastic disk was propped up against a non-flammable surface and a butane torch flame was directed at the disk from 5 cm away. The time from ignition of the torch to disk penetration was recorded. Finally, the times of the two disks were compared to each other to find which type of plastic was the most heat-resistant.

Results: When exposed to temperatures in excess of 1,400 C°, both 3-D printed disks held up much better than expected. The ABS plastic disk, which was tested first, took approximately 12 seconds for the torch flame to bore through, disproving the hypothesis. The carbon fiber plastic disk was tested next, and was able to survive over 30 seconds of constant heat without being melted through, the limiting factor being a concern over fuel consumption and overheating of the torch. This test more than proved the 3-D printed plastics worthy of being used for the intake cover, as the heat experienced during deoxygenated combustion would be much less intense and for a shorter period of time than what they were subjected to here. Due to

the clear advantage of carbon fiber over ABS plastic, it was decided that it would be used in the final prototype, though both would have been up to the task.

Prototype 1: Deoxygenated Compressor Start-up

Introduction: In the early stages of the experiment, it was soon realized that a prototype would be necessary to test the unproven concepts on which the DAST engine would rely. This initial prototype would also give insight into the difficulty of constructing a fully functional model of the engine. The primary scientific questions to be answered by this test would be, 1: Is deoxygenated combustion a feasible method of compressor start-up? 2: Can common materials, such as steel, withstand the temperatures of combustion? 3: Can a turbine and bearings made from common materials be subjected to extreme angular velocities without major mechanical failure? And 4: Would the engine and later prototypes be financially realistic? The answers found in this test would influence every descision thereafter, making it possibly the most significant component of this entire experiment. For this reason, it would be necessary to design this test with the utmost attention to detail.

Methods: To answer all three of the scientific questions, a simple solid fuel turbine would have to be designed, built, and tested. Since the test focuses around deoxygenated compressor start-up, incorporation of compressor blades was not necessary. A turbine, however, was needed to induce movement in the turboshaft for RPM measurement. A design was drafted which identified all parts that needed to be manufactured and their specifications. (fig. 4) It also included standardized fasteners for ease of assembly. This would serve as the primary blueprint

for prototype 1, but there would be some deviation from this during construction. Before gathering materials for construction, it would be necessary to define what benchmark the engine would have to perform at for the deoxygenated start-up to be considered feasible. While researching this topic, it was found that turbojet engine start-up RPM was about half that of idling (Jafari, 2019) and that model turbojet engines idle at approximately 50,000 RPM (Salt, 2021) Due to the partially-oxidized fuel grain, this would additionally reduce the required compressor intake by about one half. From this information, it was deduced that the turbine would be spinning at around 12,000 RPM before the intake cover could be separated. This meant that prototype 1 would need to accelerate the turbine to comparable speeds within the span of several seconds (or roughly 10% - 25% of the engine's total running time) to be considered feasible. To save on expenses, the body of the prototype was constructed from a soup can (which used 1/64 inch stainless steel) From the beginning there were questions as to how structurally sound this would be, especially when exposed to combustion temperatures, but it was decided that it would be used anyway. The turbine and a portion of the turboshaft assembly were made from a 1/64 inch galvanized steel sheet, which posed similar concerns. 1/8 inch dry-running plain bearings as well as a 1/8 inch carbon steel rod were purchased from the supplier, McMaster-Carr, both being used in the turboshaft assembly. After a realization that a higher turbine efficiency could be achieved through the constriction of exhaust gasses, the fan-shaped turbine design (as shown in fig. 4) was modified to a connecal design (as shown in fig. 6) A slight camber was also given to the turbine blades so that they would provide a higher torque. Because the measurement of RPM was essential to this experiment, a laser tachometer was purchased along with reflective tape. A 2" diameter disk was painted black and a strip of the reflective tape was applied to its surface with the intention of using it as a tachometer reflector.

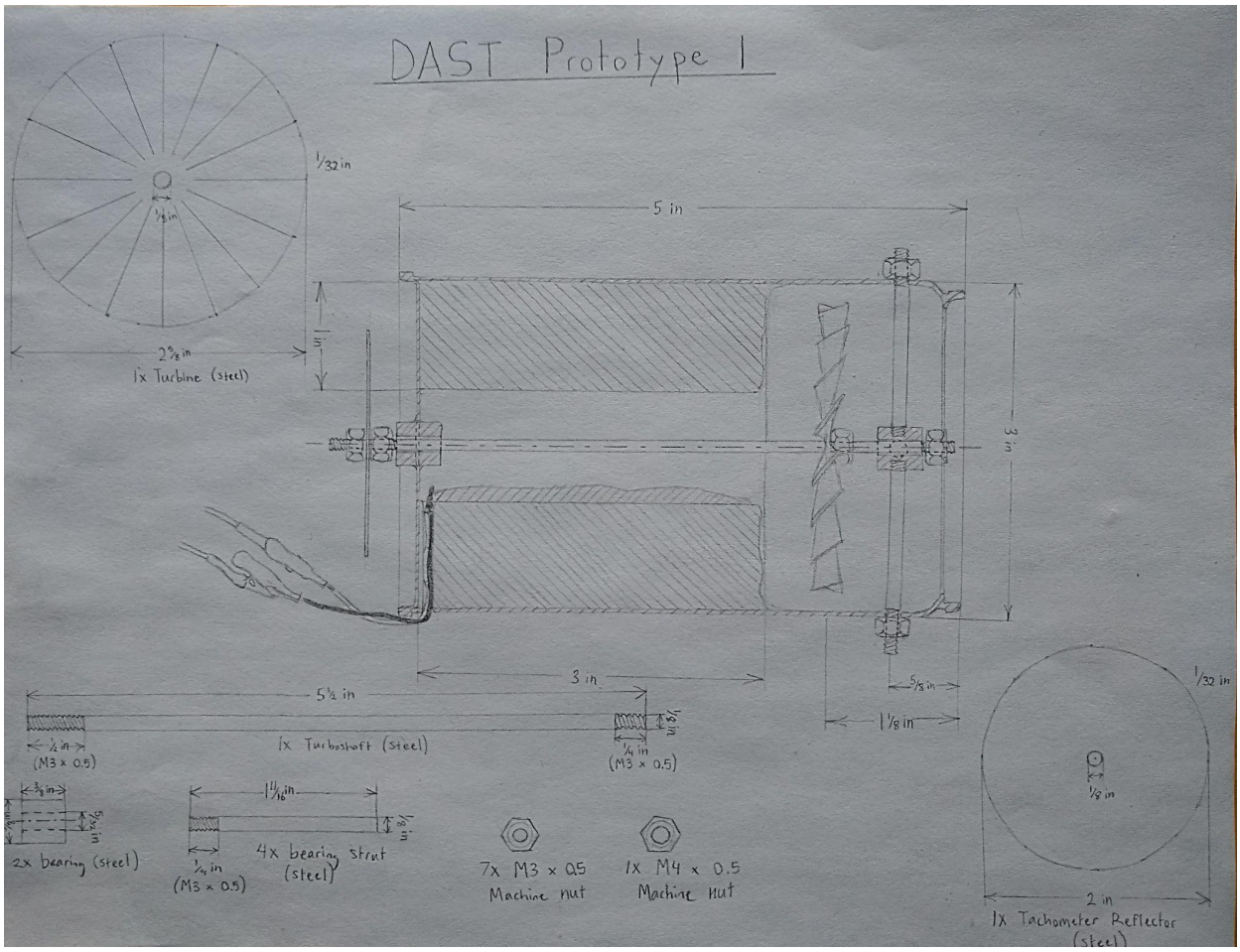

Figure 4.

Diagram and Individual Part Blueprints for Prototype 1.

To calculate how much fuel would be required for the engine, the density of the fuel was first determined. Through pouring the fuel into a vessel with a known volume and dividing the mass by volume, it was found to be 1.8 g/cm^3. From here, the volume of the fuel grain in the engine was calculated using $(\pi r_1^2 - \pi r_2^2)h$ where r_1 equals the radius of the fuel grain and r_2 equals the radius of the fuel grain bore. This yielded 238 cm^3, and when multiplied by 1.8 g/cm^3, gave 428 grams of fuel in total. Because the chosen fuel mixture was a 1:1 ratio of KNO_3 to

sugar, approximately 214 grams of each chemical would be used. After seeing this figure, there was some concern over the time it would take to mill the KNO_3 to a fine powder using a mortar and pestle. Before casting the fuel, several holes were drilled into the engine casing which would be used to fasten the turboshaft bearing and struts. A bracket was then bolted into the side of the can, serving as a method of fixing the engine to the testing base. After this, the KNO_3 was milled in a mortar and pestle, taking approximately 3 hours over the course of a two day period. The KNO_3 was then gently mixed into the confectioner's sugar using a spoon. After this point, serious precautions were taken to prevent accidental ignition of the dry fuel. A small fire extinguisher was placed nearby, and all sources of flame, such as lighters and torches, were eliminated. A paper cylinder was made and glued to the bottom of the engine casing, with its purpose being to serve as a mold for the fuel in its liquid state. It was decided that the dry fuel would be melted down in two batches, so as to prevent a major disaster from occurring on the chance that the fuel ignited during heating. Half of the fuel was added to a small saucepan, which was placed on an electric burner set at medium heat. The dry fuel was slowly stirred until completely melted to a consistent texture. The fuel was then poured into the engine, with the paper mold maintaining its shape. This was done again with the second half of the fuel, topping off the mold. After being left to cool and solidify for an hour, the paper mold was ripped away from the fuel grain, revealing a fairly symmetrical grain bore (fig. 5). Afterwards, a second 1/8 inch bore was drilled into the side of the fuel grain through one of the previous casing holes, with the intention of using it to insert the ignitor.

Figure 5.

Solidified fuel grain after removal of paper mold.

While researching types of bearings further, it was discovered that dry-running plain bearings were not suitable for rotation speeds exceeding 5,000 RPM. With prototype 1 being expected to reach speeds of 12,000 RPM, the unsuitability of plain bearings was realized and a pair of 1/8 inch steel ball bearings was ordered from McMaster-Carr. To assemble the turboshaft components, J-B Weld two-part epoxy was purchased and used to cement the turbine in place on the turboshaft as well as the two cones on either side. There was some initial concern over the strength of the glue in high-temperature environments due to an apparent flammability, but it reportedly had the highest heat tolerance out of any other adhesives that were available, at 300° C, so this was neglected. After the ball bearings arrived in the mail, sliding them onto the turboshaft was found to be an impossible task (most likely caused by the threadings on either end of the turboshaft) To remedy this problem, the threads were sandpapered down. There was little concern as to how this would affect the structural integrity because the bearings no longer relied on the nuts as end caps as they did with the plain bearings. The J-B Weld was applied to the

bearings on either end of the turboshaft, which was then affixed to the engine. The four struts were then inserted into their respective holes in the engine casing and attached to the aft bearing, with nothing but the J-B Weld to hold them in place. There was also concern here over reliance on the adhesive for such a structurally integral part of the engine, but with little other options, it would have to be made do with. After the strut adhesive had set, the tachometer reflector was secured to the end of the turboshaft by sandwiching it between two nuts with additional J-B Weld applied to the joint. Next, the dynamic balance of the turboshaft would need to be optimized to reduce any wobbling that might occur. The turboshaft was spun freely and any tendency to speed up on one side was noted. To counterbalance this, several segments of a paperclip were glued to the opposite side of the turbine. After the glue had dried, the increase in dynamic stability was clearly visible.

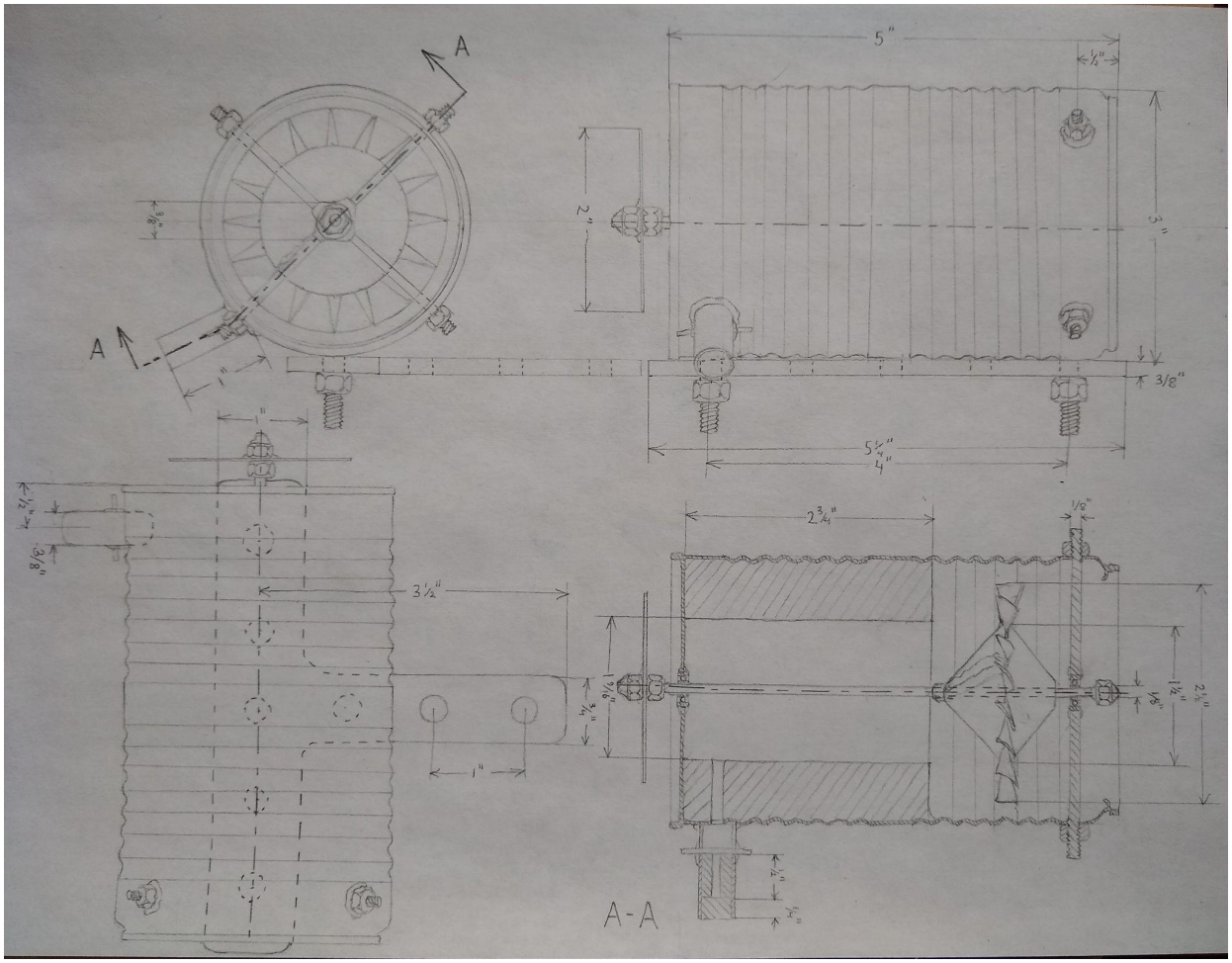

Figure 6.

Orthographic diagram of completed Prototype 1 as tested.

Igniter development: It was decided that the testing window would be held between February 19, 2022 and February 20, 2022 due to a vacation to Cape May that had been planned on the corresponding dates. Because this was learned on short notice, there would not be enough time to order rocket igniters from a supplier before departure. A prototype igniter would have to be designed and tested within a two-day period so that the window could be met.

The Estes launch controller, which was the chosen method for engine ignition, uses 6 Volts to induce an electrical current through the high-resistance igniter filament (usually

nichrome). This causes the wire to heat up, consequently igniting the fuel in close contact. Due to the resistance of the chosen fuel mixture to combust readily, an intermediary stage would be necessary, such as a black powder charge. Keeping this in mind, 3 types of wire were tested for their ability to ignite black powder, not the fuel grain. The 3 types chosen were tin foil, staples, and steel wool. First, 1 cm long samples of each wire were collected and straightened. Then a small amount of black powder was placed between two strips of clear tape and a small slit sliced in the middle with an exacto knife. The sample of wire was then inserted into the slit and clipped at either end by the jumper cables connected to the launch controller. The safety key and launch button on the controller were both depressed, and any ignition of the black powder charge would be recorded. This was done with each of the three wire samples.

With the aluminum strip, it was found that it broke almost instantaneously upon introduction of an electrical current, not providing enough time for the fuel to ignite. Additionally, the aluminum required a strip thickness of no more than 0.3 mm in diameter, which was exceedingly difficult to achieve by hand. This was most likely due to the low electrical resistance of aluminum, with the thickness of the strip being mandatory for any substantial heating to occur. When the flattened staple was tested, no apparent change occurred when being introduced to electrical current. The staple could even be touched during this process without any noticeable difference in temperature. This likely resulted from the relatively large thickness of the staple, at approximately 0.005 cm^2, cross-sectionally. Finally, with the testing of the steel wool strand, ignition of the black powder charge occurred almost instantly, with approximately a 0.25 second delay. When observed more closely, the strand was seen to glow a bright orange, indicating its high temperature. Compared with the thickness of the staple, the steel wool strand was roughly 10 times thinner, at 0.0005 cm^2. This would ultimately cause more electrical energy

to be transferred through the material per mass, resulting in a higher release of thermal energy. Because of this, steel wool strands were found to be an ideal filament for the pyrotechnic igniters.

The final design of the ignitor closely resembled a solid rocket motor in terms of function and appearance, which can be seen clearly in the A-A section of fig. 6. It was intended to work by diverting hot exhaust gasses from the ignition charge into a bore on the side of the engine, which would therefore ignite the primary fuel grain in the engine. To manufacture the ignitor, Confectioners' sugar and black powder were packed into a 9 mm paper tube, and a core was drilled through the black powder grain to increase surface area. A 2 cm long segment of steel wool was inserted into two slits on the paper tube and was glued into place with the J-B Weld to ensure contact between it and the black powder. Even the slightest gap could cause an ignition failure, and consequently, a hazardous situation to deal with. For this reason, securing the filament was an extremely important measure to take.

Finding a proper test site was crucial for the success of this experiment. Requirements included an open space with low vegetation, far from any residential area. Minimal pedestrian traffic would also be ideal. At first, remote parking lots seemed to be the primary contender, but due to a lack of seclusion, this idea was disposed of. One specific location considered was the demolished magnesite plant in Cape May Point, NJ. (Coordinates 38.945 N, 74.966 W) The sparse plant life combined with the concealed position made it an optimal choice. Additionally, Cape May Point has a permanent population of approximately 100 residents, making an unwanted encounter extremely unlikely. As was stated previously, a vacation to cape may was planned between February 19, 2022 and February 20, 2022, which made this the ideal time to test the prototype.

Test procedure: In preparation for the test, the magnesite plant was scouted for a specific testing site. An area on the Northeastern side of the plant at 38.94542 N, 74.96354 W was chosen for its lack of vegetation and relatively level surface consisting of mostly magnesite gravel. Afterwards, the ignitor which had been manufactured previously was cemented to the side of the engine using J-B Weld and allowed to dry overnight. An 18” x 24” plywood board was used as the testing base and had several holes drilled in it to accommodate the engine bolts and bracket screws. Batteries in the launch controller were replaced to ensure a successful ignition and a piece of steel wool was used to test the new batteries. A telephoto camera was also procured so that 50 FPS high definition testing footage could be recorded from a distance and analyzed. In terms of safety procedures, it was decided that safety glasses would be worn to shield the eyes in the possibility that material was violently ejected from the engine. In addition to the glasses, two fire extinguishers would be brought to the testing grounds. On the day of testing, the engine was affixed to the base via wood screws, ensuring that there would be no unwanted movement. A list of the required testing supplies was drafted, and included the following:

1. Engine
2. Testing base
3. Launch controller
4. Mobile phone (fully charged)
5. Camera stand
6. Telephoto camera
7. Drinking cup

8. Water bucket
9. Fire extinguisher (primary)
10. Fire extinguisher (secondary)
11. Launch controller base
12. Laser tachometer
13. Duct tape
14. Screws and washers
15. Screwdriver
16. Hammer

It was initially planned to assemble the engine to the base at the testing site, which explains why the engine, base, and screws are listed as separate entities. This decision was changed to streamline the field procedures. 3 experiment assistants were briefed on their roles pertaining to the test and aided in ferrying equipment to the test site via automobile. After parking in a relatively empty lot near the plant, the equipment was carried on foot to the testing site specified above. For set-up of the experiment, the engine and base was placed on the ground facing West and secured with a large stone. The telephoto camera was attached to the stand and placed aftward of the engine at a 45° angle, so that any visible turbine movement could be captured on video. It was distanced approximately 5 meters from the engine so the camera would not be damaged by hot exhaust gasses. The laser tachometer was placed directly forward of the engine at about 25 cm distance and duct taped to the wood base to minimize any movements from possible vibrations. To reduce any effect that the ambient lighting would have on the test recordings, a large stone was propped up near the base to be used as a sunshade. With the

tachometer setup in working order, the method for recording the readings was put into place. This involved mounting the mobile phone in a drinking cup and positioning it just behind the tachometer so that the digital display could be captured by the phone's 30 FPS video camera. Though the tachometer had a function that enabled the highest, lowest, and last RPM readings to be viewed following the test, there would be no way of determining when the highest velocity was reached. This could only be achieved through the use of a video camera. To start the tachometer readings a hammer was placed over the test button and duct taped in place to maintain the constant depression required to actively capture readings. After this, the 20 ft ignition cord was unraveled from the launch controller and strung between the engine and the launch controller base. The safety key was removed from the controller to prevent any accidental ignition and the jumper wires near the engine were clipped to the steel wool protruding from the ignitor. With this, it was now possible for the engine to be ignited via controller. Both the telephoto and phone cameras were activated and at this point, started capturing testing footage. The experimenter returned to the launch controller and re-inserted the safety key, announcing that the arming sequence had commenced. The safety key was then depressed and a countdown sequence was initiated, starting from T minus 3 seconds. At T minus 0, the launch button was pressed, sending an electrical current through the wire to start ignition. After the engine fuel grain had been completely consumed, it was approached with a bucket of water and doused to lower the temperature and prevent any accidental fires from occurring. In the event that the test ignited a bushfire, the two dry chemical extinguishers would be utilized. The two video cameras were deactivated and when it was absolutely certain that any combustion had been extinguished, the tachometer and mobile phone were removed from the testing base and packed away with the

remaining field supplies. While the supplies were retrieved for reuse, the engine and base were transported from the testing site to be studied.

In the first step of data collection and organization, the phone camera footage was viewed to recover the laser tachometer readings, with data points being recorded every 0.2 seconds of operation. These points were then applied to a graph of turbine angular velocity over time for a better visualization. To corroborate this data recorded by the tachometer, the phone video footage was closely analyzed, with careful observations being paid to the dynamic geometries formed by the reflector strip. Specific measurements were derived from this analysis through comparison with the video frame rate of 30 FPS. As a final confirmation of the maximum angular acceleration of the turbine, a tone generator (Szynalski, 2012) was used to determine the highest audible frequency created by the engine. This frequency in Hertz was divided by the number of blades (16) due to the hypothesis that there would be a pressure oscillation for every blade. This in turn would produce 16 oscillation periods per revolution, helping to to determine the angular velocity. From here, the angular velocity rate of change was found to determine if the turbine could reach the benchmark speed of 12,000 RPM in an appropriate amount of time. After this, the physical condition of the engine was recorded so that any damage sustained during the test could be analyzed for a probable cause. The engine was then disassembled, taking note of any fastinings that had failed or accumulation of combustion byproducts. Special attention was paid to the turbine to see if any deformations had occurred due to overheating or centrifugal force acting on the blades. The condition of the bearings was also evaluated for any indication of failure. The telephoto footage was then closely analyzed, identifying significant events in the test and counting frames of duration before dividing this by the frame rate. This would aid in compiling highly accurate timestamps for a chronological record of the test. This record, along

with the graph of angular acceleration, were used in conjunction with the information gained from the disassembly, and an interpretation of the test results was derived.

Results: Before casting, the mass of the engine casing was found to be 112.7 grams, but after the addition of fuel, this increased the total mass to 467.8 grams. Finding the difference between these two values, this gave the propellant mass, which was calculated at 355.1 grams. Because the initial mass of the chemicals used was 420 grams, this meant that there was a 64.9 gram loss throughout the process of fuel production, or 15.45%. In future prototypes, this loss of fuel will be accounted for beforehand, with the quantities of fuel being adjusted accordingly. The completed turboshaft assembly had a mass of 40 grams, along with the bearing struts, which had a collective mass of approximately 10 grams, though this is not confirmed. All together, this added an additional 50 grams to the engine, resulting in a total full mass of 517.8 grams, or just over 1 pound.

The process for affixing the turboshaft assembly to the engine and struts was riddled with complications, most of which stemmed from the use of J-B Weld. While waiting for the parts to set in place, some of the J-B Weld contaminated the ball bearings. This required immediate removal of the turboshaft and immersion in an alcohol solution to ensure that the bearings weren't permanently damaged. When a second attempt was made to install the turboshaft, there was a great difficulty in keeping the whole assembly stationary while the adhesive set. Some effort was made to prop the turboshaft into position with wooden sticks, but this failed. Finally, hot-melt adhesive was used to temporarily stabilize the turboshaft struts, and this worked excellently. Next morning the hot-melt adhesive was peeled off of the struts, which held their position with the J-B Weld set in place.

The evening before the test of prototype 1, when the 2 gram ignitor was being cemented to the external port on the engine, it was found that the angle at which the port had been drilled (45°) was too low, causing the ignitor to protrude too far downward. This would severely impede fastening the engine to the testing base and for this reason, a solution was investigated. One idea devised was to cut part of the ignitor's paper tube so that the junction between it and the engine casing would be slightly angled. When applied, this reduced the ignitor's angle relative to the base, allowing the engine to be properly fastened down. Because of the overall inconvenience, it was noted that in following prototypes, the ignitor port would be drilled horizontally or possibly upwards at a 45° angle.

After the engine had been completely assembled, a list of all the materials used was compiled, as well as the prices that would normally be paid for them. The price actually paid for each material was also recorded, as the vast majority were obtained without any expense. Because the cost to manufacture each unit could prove to be valuable information given the prototype was ever mass produced, the general price was broken down into the quantities of each material actually used and their subsequent cost. This information was all organized into Table 3, as shown below.

Table 3.

Cost of all materials obtained and/or used in the construction of Prototype 1.

Materials	Market price (USD)	Actual expense paid (USD)	Price of used materials (USD)
1 soup can	1.17	0	1.17
1 ft^2 1/64" galvanized steel	7.03	0	0.78

2 ball bearings	14.06	14.06	14.06
1/8 x 24 steel rod	15.80	15.80	8.51
J-B Weld steel reinforced epoxy	14.88	14.88	1.00
100 6-32 nylock nuts	6.40	0	0.58
50 1/4-20 x 1 machine screws	11.19	0	0.45
1lb Spectracide stump remover (KNO_3)	5.89	0	2.72
2lb confectioner's sugar	2.79	0	0.65
1 aluminum bracket	3.66	0	3.66
12 reflective tape strips	8.99	0	0.15
3 steel wool scrubbers	2.48	0	< 0.01
1 ream of paper	4.77	0	0.01
1lb sulfur plant fungicide	7.49	0	< 0.01
Flat black acrylic paint	3.40	0	0.15
Total	110.00	44.74	33.89

When the final ignitor preparations were being done for the test of prototype 1, several tests of the steel wool filament were conducted. These tests consisted merely of running an electrical current through the strip to analyze thermal heating characteristics in different

circumstances. It was found that the strips experienced some difficulty maintaining temperature in cold environments, which added concern for the reliability of ignition during the prototype 1 test. Additionally, it was found that the filament also experienced heating difficulty when small blobs of J-B Weld were placed on its surface (as they were in the finalized ignitor design)

The testing group departed to the magnesite plant at approximately 2:30 PM on February 20, 2022. The atmospheric conditions were completely cloudless, causing intense sunlight from the Southwest of the testing grounds. Upon arrival, the engine and testing base were placed on the ground and secured with a large stone, as written in the method. It was not, however, originally planned to use a sunshade for the tachometer, as no difficulties in obtaining readings were anticipated beforehand. Because of this, when the tachometer was activated, it was discovered that the laser didn't detect enough contrast between the reflective strip and black paint, and was therefore unable to create measurements. This was a significant cause of concern, as effectiveness of the experiment relied heavily on the accurate readings provided by the tachometer. It was deduced that this lack of contrast between the paint and reflective tape was caused by the intense ambient light, which prevented the photosensor from isolating the reflected laser signals. To remedy this effect, the engine and base was rotated 180° so that the engine was facing East, and was consequently in shadow. When tested again, the same effect was observed, most likely due to light being reflected by the chalky magnesite rubble. The engine and base was rotated back to its original position, and this time a large stone was propped up near the base to be used as a sunshade. It was theorized that the shadow cast over the reflector disk would increase contrast, and when the tachometer was activated, this was proven to be correct. Though this worked as a temporary fix on the testing grounds, a more permanent solution in further prototype tests would be discussed later on in the paper.

After the experiment setup had been partially completed, it was realized that the water bucket, which was the first resort for fire extinguishment, had been forgotten. As the setup was completed, two assistants departed to retrieve the bucket, and on their return, the test of prototype 1 could commence. When both the phone and telephoto cameras were started at 2:54 PM, the arming and countdown sequence was initiated, however, attaching the jumper wires to the ignitor had been overlooked during the experiment preparation, causing ignition failure. This was soon realized, and when absolutely certain that no discharge of electrical current had occurred and that the controller was disarmed, the engine was approached and the wires were clipped to the steel wool filament. This operation can be seen between 30 and 53 seconds in the telephoto video footage.

After the wires had been secured to the ignitor, the arming and countdown sequence was reinitiated, with time of ignition being set at 1 minute and 4 seconds into the footage. The launch button was depressed on T - 0 seconds, with the first visible signs of ignitor grain combustion appearing at T + 0.37 seconds. This was shortly followed by breakage of the ignitor filament, which caused the wires to quickly recoil due to tension. This breakage was most likely the result of high electrical current combined with heat from the ignitor grain, and did not at all negatively affect the results of the experiment. The ignitor grain continued burning successfully for 0.93 seconds, diverting the hot exhaust gasses into the ignitor port with no blowout or unintentional diffusion of combustion pressure being observed. After the ignitor charge was completely depleted, smoke could still be seen billowing out of the engine exhaust opening. This was likely caused by the main fuel grain beginning to combust, and in this stage, the thrust and burn rate produced by the engine could be considered negligible. Over the next 2.77 seconds, it can be deduced that the area of combustion grew at a mild rate, spreading from the ignitor bore to the

interior surface of the grain. At this time, the laser tachometer began displaying a reading of 344 RPM, however this was clearly incorrect as movement in the turboshaft appeared negligible in the footage. This false reading was most likely caused by the copious amounts of smoke created during the test, which would have caused significant interference with the tachometer reflector. Because of this discovery, the measurements of the laser tachometer were largely disregarded, and visible reflector geometry recorded by the phone camera was now the primary method of angular velocity measurement.

Table 2.

Raw data of turbine angular velocity and time.

Time (seconds)	Angular velocity (RPM)
0	0
0.2	25
0.4	50
0.6	300
0.8	720
1	1,260
1.2	1,950
1.4	3,150
1.6	4,050
1.8	4,950
2	5,400
2.2	5,950
2.33	6,300

2.4	5,400
2.46	3,600
2.53	1,800
3	900
3.2	300
3.4	150
3.6	0

At T + 4.07 seconds, the first signs of turboshaft movement became apparent in the phone camera footage. This closely reflects the corresponding frames of the telephoto footage, as a large billow of smoke can be seen at this time, followed by an extreme increase in exhaust velocity (viewed by flying particles). This indicates a dramatic increase in combustion area and mass flow rate, as the rate of combustion is directly correlated to exhaust velocity. It can be observed in the footage that as a result of the initial sluggish burn rate and exhaust velocity, opaque smoke was produced, but as the burn rate hastened, the exhaust smoke became transparent because of the flow rate increase. Within the first 0.4 seconds of turboshaft acceleration, the angular velocity slowly climbed to 50 RPM, and then made a jump to 300 RPM in the next 0.2 seconds, as shown in table 2 and fig. 8. This meant that the initial angular acceleration of 125 RPM/s increased to 1,250 RPM/s after approximately the first half-second, with angular acceleration being linearly correlated to the torque exerted on the turboshaft. Due to the increasing exhaust velocity during the test, torque produced by the turbine blades rose exponentially (specifically to the power of 2), as per the equation of lift. This caused a rapidly increasing rate of angular acceleration in the turboshaft (represented in the first 1.5 seconds of fig. 8) with the angular acceleration climbing from 3,450 RPM/s (361 Rad/s^2) to 6,000 RPM/s

(628 Rad/s^2) in 0.2 seconds. After this point, however, angular acceleration of the turbine declined for an unknown reason, forming a set of data which conformed more closely to a sine wave than the originally hypothesized exponential equation. Additionally, as the fuel grain combusted, the steel of the engine casing went through a process of discoloration, becoming significantly duller. This was likely due to a chromium-oxide layer building up on the engine as it was heated. At about T + 5.6 seconds, a high-pitched sound was emitted from the engine, the origin of which most likely being rotation of the turbine. As the turboshaft angular velocity climbed from 2,550 RPM, so did the frequency of the sound produced, further supporting this hypothesis. Though not originally intended, it was deduced that the maximum frequency of the sound generated by the turbine could be used to corroborate the data obtained from the video footage. At T + 6.4 seconds (2.33 seconds into turboshaft movement), the highest measurement of turbine angular velocity was recorded, with a reading of 6,300 RPM. The sound produced at this instant was approximately 1,680 hz, and when converted to RPS using the calculations mentioned in the method, the exact same angular velocity value was found, perfectly corroborating the visually derived data.

Turbine Angular Velocity Over Time

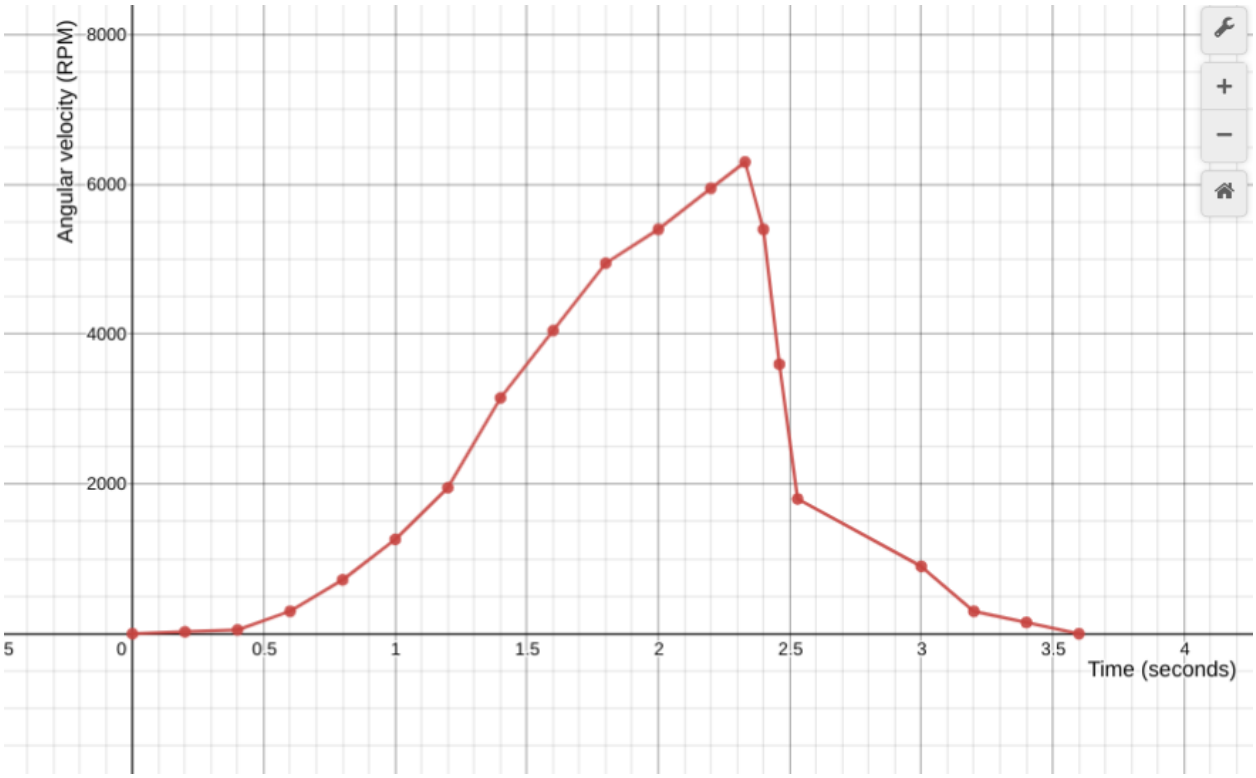

Figure 8.

Angular velocity of the turboshaft graphed from initial movement. (T + 4.07 seconds)

The last recorded value of angular acceleration was 2,690 RPM/s (282 Rad/s^2) before movement of the turboshaft was violently interrupted. This sudden disturbance resulted in the turbine angular velocity dropping from 6,300 RPM to 1,800 RPM in just 0.2 seconds, which is also represented in table 2 and fig. 8. At the same time, the mounting bracket for the engine could be seen to lift approximately 2 mm off the base before slamming back into place, slightly disrupting the phone camera's positioning with the jolt. Additionally, several very large pieces of what were likely combustion deposits being ejected from the engine at high speeds can be seen in the telephoto footage. (fig. 9) Soon after the rapid deceleration of the turboshaft, the exterior

fasteners connected to the bearing struts could be seen separating from the engine casing and rattling in place, indicating that the J-B Weld had failed, possibly in multiple areas. 4.67 seconds later, the ratting ceased, coinciding with a visible change in the exhaust smoke pattern, which began rotating counter-clockwise as seen from behind. Finally, the exhaust velocity slowed, eventually concluding fuel grain combustion at T + 17.74 seconds. This meant the majority of the fuel grain was consumed in a time interval of 13.64 seconds. As the exhaust gasses dispersed, the throat of the engine produced a small orange flame. This was caused by an unintentional ignition of the polymer-based J-B Weld, and was soon extinguished when the engine was approached and doused with a bucket of water. Other than this, no additional instances of unintentional fires occurred during the test. When collecting the recording instruments, it was found that both the phone and telephoto camera had successfully captured their respective footage and were powered off. This concluded the test of Prototype 1.

Figure 9.

Debris being ejected from the engine soon after turboshaft dislocation.

Upon initial inspection, it was seen that while the exterior of the engine was relatively unchanged, the turboshaft and other internal components had been displaced and malformed. Shown in fig. 10, the displacement of the turbine is extremely visible as well as the separation of the aft cone. This clearly indicates that the J-B Weld failed, as anticipated. In addition to the turboshaft structures separating from each other, the entire turboshaft became dismounted from the bearing struts with the reflector disk pressing into the front exterior of the engine. The reflector disk, itself, had been superficially damaged to the point where it would not be able to serve its intended purpose. The reflective tape strip had fallen off and the black paint had been weakened so that large sections flaked away, though the overall structural integrity of the disk had not been compromised.

Figure 10.

Photograph depicting the interior of Prototype 1 following testing.

When the engine parts were removed for a more in-depth analysis of their condition, it was found that the turbine blades had been slightly angled in a counter-clockwise direction, though they were relatively undamaged. This can also be seen in fig. 10, along with circular scratches on both the turboshaft cone and turbine. There was almost no remnant of J-B Weld adhesion on the interior of the engine where it was used copiously, with the only exception being joints between the turboshaft and bearings. However, there was a significant accumulation of carbon deposits inside the engine casing and on the turbine blades, with the layer being as thick as 1 cm in some areas. The only components that were spared from the deposits faced aftward of

the engine. Closer inspection of the ball bearings showed that both of them were completely locked in place and unable to be rotated, though it was unsure when in the test this occurred. A conclusion to this vital question would be drawn in later analysis. Besides the ball bearings being permanently damaged, there was no other significant structural damage to the parts.

Discussion: The manufacturing of Prototype 1 demonstrated several important concepts which could prove to be invaluable later on in the experiment. Firstly, it showed that the simple methods used for shaping and joining the parts of the engine were effective and could be done with minimal equipment. This is important because one of the main goals of this experiment is the reduction of complexity and manufacturing price in turbojet engines. Additionally, it showed that manufacturing methods would not need to be majorly revised, with the one exception being the way in which the J-B Weld was utilized. Financial analysis of the data provided in Table 3. shows that the manufacturing of Prototype 1 was extremely economical when compared to other types of engines, even being priced below some similarly sized solid rocket motors. While the total market price of all materials was fairly expensive, at 110.00 USD, this is an abstract unit, with values being largely dependent on the quantities which were bought. The actual cost expended to make the engine came to 44.74 USD, which is less than the total market price, but can also be neglected on the basis that it is only accurate for the specific conditions in which the experiment was conducted. The availability of certain materials could vary greatly depending on the circumstances, and therefore should only be regarded as the experiment price. For estimating the cost it would take to mass produce the Prototype 1 design, the total cost for the price of used materials is much more accurate, at 33.89 USD. This is the primary cost value to be referred to, as it is least likely to vary depending on the experimental conditions.

From the results of the experiment setup at the testing grounds, it can be drawn that there wasn't sufficient information on the environmental conditions and how they would affect the experiment, specifically the tachometer. This led to last-minute attempts at achieving a functional configuration, and while ultimately successful, delayed the experiment and added unnecessary concern. To have prevented this problem, preliminary tests involving the tachometer should have been conducted. This would have allowed identification of the issue, as well as the creation of possible solutions. In future prototypes, a more permanent solution that was hypothesized would utilize PVC pipe to act as an extended sunshade. This would ultimately close the photosensor's field of view, allowing it to detect smaller contrasts in laser reflection. The initial issue with tachometer data collection ties into the overarching lack of preparedness at the testing ground, with multiple steps in the experimental process being overlooked. A more general solution for this would be to have a procedural checklist. Though there had been a supplies checklist brought to the testing site, it did not specify the different tasks that were to be carried out in preparation for the experiment. Having a procedure list could have streamlined this complex process greatly, and will definitely be utilized in the testing of future prototypes.

In regard to analysis of the actual test results, the ignitor performed very well, in fact better than hypothesized. The time delay between controller input and ignition was fairly short, at 0.37 seconds. This would allow ignition to be precisely regulated, and could prove to be applicable for prototype tests where multiple timed ignition events would be necessary. Specifically, it showed that precise timing and detonation of the intake cover in final DAST prototypes would be feasible. On the effectiveness of igniting the main fuel grain, the ignitor again displayed its effectiveness. Here, there was some question as to whether the 1 gram of pyrotechnics would be able to ignite the fuel grain, which was weakly oxidized and had a

comparatively low surface-area to volume ratio. Despite this, the ignitor was still able to cause the fuel grain to begin combusting.

Simultaneously to initial fuel combustion, the laser tachometer began to give readings that were clearly false, such as the measurement of 344 RPM when the turboshaft was completely stationary. Readings like this proved that the tachometer was unreliable for obtaining accurate data on the testing of Prototype 1, however, it could still be valuable for use in later prototype tests. The factor that caused this malfunction was identified as the copious amount of smoke interfering with laser reflection, and it was reasoned that this interference could be reduced through use of the PVC pipe mentioned earlier. With the modification, it would allow the tachometer to collect much more reliable data due to reduction of smoke from the line of sight as well as reduction of ambient light, two key advantages.

Due to the moderate amount of smoke that was produced by the engine between T + 1.3 seconds and T + 4.07 seconds, it was reasoned only a small amount of the interior fuel grain surface area was combusting at this time. The location of combustion can be traced to the ignitor bore, where it lingered before spreading rapidly to the main core at T + 4.07 seconds. At this point, the turboshaft began experiencing angular acceleration, which was gradual initially, at 125 RPM/s, but then became more rapid, eventually peaking at 6,000 RPM/s. As stated previously, the angular acceleration of the turboshaft was directly proportional to the force produced by the engine, and therefore the combustion area. From this, it can be concluded that the combustion area grew further, likely spreading from the forward section of the combustion chamber to the rear. This rapid expansion of the combustion area supports the idea that deoxygenated combustion would be a feasible method of compressor start-up, as peak angular acceleration

would need to be obtained as rapidly as possible. This would prevent fuel wastage during the start-up phase, maximizing the engine's efficiency.

After the initial phase of exponential angular acceleration, this rate began to decline mildly. There are several explanations as to why this happened, with the most likely being that the turbine passed its angular velocity of maximum efficiency. This would be due to the vector of exhaust gasses relative to the turbine exceeding the angle of blade inclination, which can be corroborated by the calculated exhaust velocity. A graph shown in (Winslow, 2017), demonstrates how the angle of attack can greatly affect lift values, and in the case of a turbine, torque. Another explanation for the loss of acceleration is that combustion byproducts began to accumulate on the turbine blades as seen during the inspection of the internal components, resulting in a drop in turbine efficiency. Though this is entirely possible, the deposits most likely accumulated after the turbine had stopped, as centrifugal force would have made adhesion of debris on the blades unlikely.

As the angular velocity of the turbine reached 6,300 RPM, it experienced a rapid deceleration of about 22,500 RPM/s. Because of this interruption it would be imperative to identify the cause and determine if it was valid evidence for a lack of feasibility. Close analysis of the telephoto footage revealed that the engine bracket lifting off the base coincided perfectly with the turboshaft deceleration. From this information, it was concluded that the kinetic energy stored by the turboshaft was rapidly transferred to the engine casing. This caused the engine to torque in a clockwise direction as seen from behind, jolting off of the base before slamming back down. Because energy was directly transferred to the engine, this proves that mechanical disruption was the primary cause of turbine deceleration. Though this had been assumed initially, visual confirmation provided concrete evidence that loss of combustion pressure or other

external factors were not to blame. From here, several theories were formulated as to what exactly caused the turbine disruption, with the primary theory being that the J-B Weld failed in the high-heat conditions, causing the turboshaft detach from the engine. This would result in the reflector disk slamming into the front of the engine, acting as a sort or break pad which would rapidly decelerate the turboshaft. One key piece of evidence that supported this conclusion was the condition of the turboshaft assembly following the test (fig. 10). From this, it is indisputable that the turboshaft became dismounted during the test, but the key question that still remained was *when* this happened. If it occurred after deceleration of the turbine, it could imply that the bearings or some other fundamental component had been overstrained. This would be a cause of major concern, as it might indicate that deoxygenated start-up was conceptually flawed, and therefore impractical. In the disassembly of the engine, however, two key features were discovered that disproved this. First, the blades of the turbine had been uniformly bent forwards and in a slight counter-clockwise direction. This type of deformation could only be attained through a dismount during rotation of the turbine, as nothing else would explain the blades bent opposite to the direction of rotation. The second strong piece of evidence to support this theory is the circular scratches around the aft cone and turbine, which can be seen clearly in fig. 10. These show that the turboshaft was still spinning when it became displaced, abrading against the other internal components before it came to a stop. With these two pieces of evidence demonstrating that turboshaft displacement coincided with the deceleration, it can be concluded that failure of the J-B Weld adhesive was to blame for the sudden termination of rotation. In a reconstruction of the events that lead up to this failure, the adhesive holding the turboshaft bearings had been weakened significantly by the heat of combustion, and at T + 6.4 seconds, gave way to the force being exerted on the turbine. This caused the turboshaft to slip forward off of its mountings with

the reflector disk slamming into the front of the engine. The friction created by the disk along with the turbine blades caused rotation to come to a complete stop. This analysis is significant because it indicates that no fundamental flaws existed in the design of Prototype 1, with the only failure being derived from material limitations.

Because the data collection on turboshaft angular velocity was interrupted by the adhesive failure, the maximum potential angular velocity was never determined. As this data would be necessary to identify whether or not the turbine had reached the approximated benchmark of 12,000 RPM, it created a large hole in analysis. Though this hole could be possibly filled through the test of a second prototype, it would be very time consuming. A simpler method would be to derive equations which could roughly predict the potential maximum angular velocity of the Prototype 1 turboshaft. This could be achieved using several different mathematical methods, with the most apparent being identification of trends in collected data. As mentioned above, the graph of angular velocity very closely resembled a sine wave, and in predicting the potential angular acceleration it was assumed this trend would continue. As stated previously, the reason for the decrease in angular acceleration most likely derived from exceeding the velocity of maximum efficiency. Because blade efficiency is based on the angle of the exhaust vector relative to the turbine blade, it would be logical for angular velocity to follow a trigonometric relationship. An equation was derived in an attempt to model the data set as closely as possible

$$v_{\theta} = 3500sin(1.15t - 1.75) + 3500$$

where

v_{θ} = Angular velocity (RPM)

t = Time (seconds)

As shown in fig. 11, the vertex of the equation lies at the coordinates (2.89, 7000). This indicated that the turboshaft of Prototype 1 would take 2.89 seconds to reach maximum angular velocity, which would be approximately 7,000 RPM. This estimated angular velocity is not quite as much as the benchmark of 12,000 RPM, which raised some concerns. Though the benchmark was initially designated as a threshold of feasibility, it also was formulated using very rough approximations. Additionally, the turboshaft's maximum angular velocity cannot be completely determined until a second prototype has been tested. While this estimated maximum angular velocity was slightly lower than the specified requirement, the approximate time to reach that velocity would exceed expectations, at 2.89 seconds. In this duration, only 21% of the fuel would be consumed, reserving the rest for efficient oxygenated combustion.

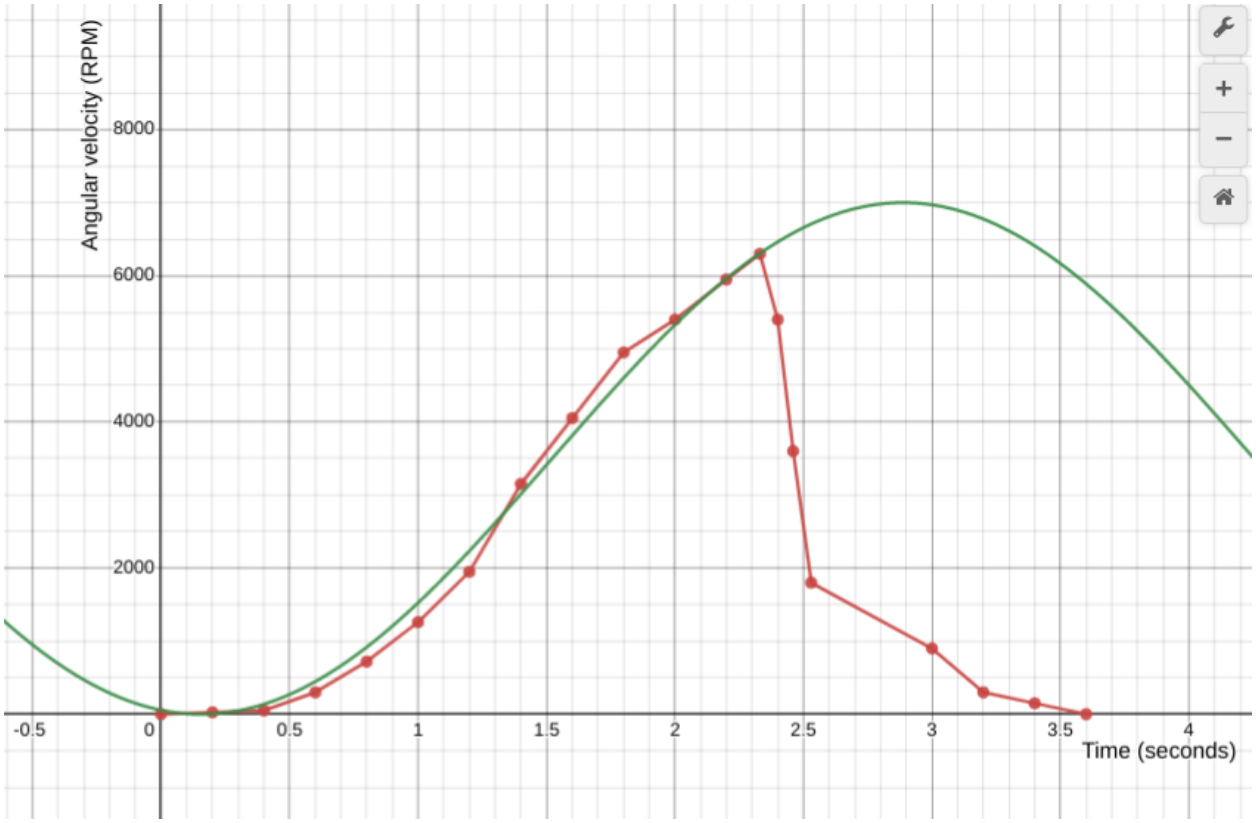

Figure 11.

Turboshaft angular velocity graphed with corresponding trigonometric equation.

For further confirmation of the angular velocity estimate a second mathematical method was utilized. Instead of relying heavily on trend identification, however, this method would utilize mechanical physics. Since it is known that the angular velocity of a turbine is limited by fluid flow rate, it would be possible to calculate the maximum theoretical velocity of the turboshaft using exhaust velocity. For this to be done, the exhaust velocity would have to first be calculated. All the known variables were specified below

where

I = Moment of inertia

m = Turboshaft mass

r = Turbine radius

τ = Torque

Δv_{θ} = Angular acceleration (Rad/s^2)

F = Engine force

L_b = Length of blade

Δm_f = Fuel mass flow rate

m_f = Fuel mass

t = Time

v_{exh} = Exhaust velocity

v_{θ} = Angular velocity (RPM)

The first equation used would calculate the turboshaft's moment of inertia.

$$I = \frac{1}{2}mr^2$$

When the known values are plugged in, this gives a moment of inertia equal to 0.0000245 kg*m^2

From here, torque exerted on the turbine could be calculated.

$$\tau = I\Delta v_{\theta}$$

This yields 0.0154 N-m of torque. Torque can be easily converted to the force, and as the lift coefficient of each turbine blade is roughly equal to 1, no conversion is necessary to find the engine thrust.

$$F = \frac{\tau}{r - \frac{1}{2}L_b}$$

The resultant engine thrust is equal to 0.56 Newtons. While this value was unexpectedly low, it most likely was the result of a weakly-oxidized fuel grain and interference from the turbine. Finally, after finding the mass flow rate, the exhaust velocity of the engine can be calculated.

$$\Delta m_f = \frac{m_f}{t} \qquad v_{exh} = \frac{F}{\Delta m_f}$$

With the mass flow rate of 0.026 kg/s, and a thrust of 0.56 Newtons, the engine was found to have an exhaust velocity of 21.5 m/s. The very last step of this process is to convert this exhaust velocity to angular velocity. Since tangential velocity in a turbine is limited by exhaust velocity, that values are assumed to be the same at maximum angular velocity.

$$v_{\theta} = \frac{60v_{exh}}{2\pi(r - \frac{1}{2}L_b)}$$

After solving this final equation, the maximum angular velocity is found to be 7,466 RPM. This value is fairly close to 7,000 RPM, corroborating the initial estimate derived from data trends. The similarity between the two estimations demonstrates that both are likely accurate, providing

substantial evidence that the turboshaft still wouldn't have reached the benchmark had it been uninterrupted. Though this is true, it is not large enough of a discrepancy to dismiss deoxygenated start-up all together. The ability to reach an angular velocity 60% to the hypothesized benchmark can certainly be considered a success, and with design revisions made from the conclusions drawn here, future prototypes could be able to bridge this gap.

To assess whether the common materials used in construction of Prototype 1 showed any signs of weakening due to extreme heat, analysis of the internal components was key. Inspection of the turbine showed that no deformation occurred, besides the damage sustained from dismount and impact with the interior. This was surprising, as it had been hypothesized that failure of the turbine due to heating would have been almost inevitable, considering the extremely high surface area to mass ratio derived from the use of 1/64 inch steel. Further inspection of other internal components such as the turboshaft and cones additionally showed no signs of heat deformation, though it was considered that heat may have caused both of the steel ball bearings to lock in place after turboshaft deceleration. No deformation was observed externally, but due to the low design tolerances of the bearings, slight heat warping could have caused a failure. The most apparent failure during the test of prototype 1, however, was the weakening of the J-B Weld adhesive. Based on the discoloration of the engine casing viewed in the telephoto footage, the combustion chamber reached approximately 500 ° C. Due to the adhesive's temperature rating of 300° C, it failed in the high-heat conditions of the combustion chamber. This resulted in the separation of almost every internal joint, ultimately limiting the turbine's maximum angular velocity. Because of this, the most significant alteration in any future prototype would be the use of temperature-resistant fastenings, and the limitation of adhesive use within the combustion

chamber. Again, this shows that the concept of deoxygenated compressor start-up is feasible, and the only limitations were caused by adhesive misuse in the construction.

Similarly to analysis of the engine materials' response to heat, an assessment of the stress caused by the turboshaft's high angular velocity would also be necessary. Again, the internal components of Prototype 1 were inspected to identify any deformations that may have been caused by centrifugal force. As they had been exposed to combustion temperatures and were therefore more ductile, this would magnify the damage caused by centrifugal force. Despite this, no damage derived from the high angular velocity was discovered. Before the test, it was hypothesized that the turbine blades would be most likely to fracture due to the small points of connection to the rest of the turbine, and though this did not occur, it could have been possible if a higher angular velocity was attained. To calculate the angular velocity at which the turbine blades would fail, it would first be useful to calculate the maximum centrifugal force exerted during the testing of Prototype 1. This was done by formulating the equation,

$$F_c = \frac{m_b(2\pi(r - \frac{1}{2}L_b)v_\theta)^2}{r - \frac{1}{2}L_b}$$

where

$F_c =$ Centrifugal force exerted on each blade

$m_b =$ Mass of each blade,

$L_b =$ Length of blade

$r =$ Turbine radius

$v_\theta =$ Angular velocity (in rotations per second)

When the appropriate values were plugged into this equation, it yielded a force of 4.19 Newtons acting on each blade, or approximately 0.94 pounds. Given that each blade had a mass of around 0.35 grams, rotation of the turbine generated 1,220 Gs at the perimeter. This shows that the turbine performed exceptionally well given its simple construction, proving itself to be practical in extreme applications. This further supports the feasibility of a simple turbine engine.

Through careful analysis of the data collected during the testing of Prototype 1, an answer was derived for each inquiry posed in the introduction. When used in conjunction with one another, it can be concluded that the overall results of the test were extremely favorable, and far surpassed expectations. A large quantity of data analysis was used to draw this interpretation, ranging from angular acceleration of the turbine to ease of assembly, however, none of these were necessarily novel concepts. The most valuable information gained from this experiment was proof that a jet turbine can be accelerated using exclusively solid fuel, something that has never before been demonstrated before on a physical level. Aside from serving as concrete evidence that deoxygenated compressor start-up is feasible, solid fuel turbines could prove to be beneficial in countless other applications, such as power generation. In terms of next steps to take before a fully-functional prototype of the DAST engine is constructed, it would be necessary to gather more data on turboshaft angular acceleration. This is due to the testing of Prototype 1 being cut short as a result of adhesive failure. To avoid this in the next prototype, all application of J-B Weld within the combustion chamber would be avoided, relying solely on metal fasteners. Even though this failure limited the collection of turbine data from Prototype 1, the data that was collected turned out to be invaluable for the experiment as a whole, substantiating the hypothesis that a deoxygenated start-up could be achievable.

References

Fahlstrom, S., Pihl-Roos, R. (2016). Design and construction of a simple turbojet engine. *Uppsala Universitet.* https://www.diva-portal.org/smash/get/diva2:974874/FULLTEXT01.pdf

(1998). Turbine engine basics. *Purdue AAE Propulsion Page. Purdue University.* https://engineering.purdue.edu/~propulsi/propulsion/jets/basics.html

Jet engine pressure distribution. *(No original source?)* https://i.pinimg.com/originals/97/44/79/97447973a6c2d6f7cfa6be62602e87cb.jpg

Kashkhan. (2009). Specific impulse vs. mach number of several types of rocket and air-breathing engines. *English Wikipedia.* https://commons.wikimedia.org/wiki/File:Specific-impulse-kk-20090105.png#/media/File:Specific-impulse-kk-20090105.png

Li, J., Liu, K. (2018). Combustion characteristics experimental study of solid hydrocarbon propellant for air-turbo rocket. *JPP.* https://arc.aiaa.org/doi/10.2514/1.B36917

Lee, J. (2018). How to calculate time to heat an object. *Sciencing.* https://sciencing.com/calculate-time-heat-object-8223103.html

High speed aerodynamics - compressibility effects. *Flight Mechanic.* *https://www.flight-mechanic.com/compressibility-effects*

Jafari, S. (2019). Modeling and control of the starter motor and start-up phase for gas turbines. *Cranfield University*.

file:///home/chronos/u-d982e7bf94c8d13476f0657cf30af2435755f417/MyFiles/Downloads/electronics-08-00363.pdf

Salt, J. (2021). Understanding model jet engines. *RC Helicopter Fun.* https://www.rchelicopterfun.com/model-jet-engines.html

Nallard, O. (2020). Air-breathing rocket engines: the future of space flight. *Physicsworld.* https://physicsworld.com/a/air-breathing-rocket-engines-the-future-of-space-flight/

Winslow, J., Otsuka, H. (2017). Basic understanding of airfoil characteristics at low reynolds numbers. *American Institute of Aeronautics and Astronautics.* *https://arc.aiaa.org/doi/10.2514/1.C034415*

Szynalski, T. (2012). Online tone generator. *Hope This Helps.* *https://www.szynalski.com/tone-generator/*